INTERNATIONAL JOURNAL FOR NUMERICAL METHODS IN FLUIDS
Int. J. Numer. Meth. Fluids 2003; **42**:383–398 (DOI: 10.1002/fld.519)

A spectral/finite-difference approach for narrow-channel flow with inertia

Mizanur R. Siddique and Roger E. Khayat*,†

Department of Mechanical and Materials Engineering, The University of Western Ontario, London, Ontario, Canada N6A 5B9

SUMMARY

A hybrid spectral/finite-difference scheme is proposed to determine the inertial flow inside narrow channels. The flow field is represented spectrally in the depthwise direction, which together with the Galerkin projection lead to a system of equations that are solved using a variable step finite difference discretization. The method is particularly effective for non-linear flow, and its validity is here demonstrated for a flow with inertia. The problem is closely related to high-speed lubrication flow. The validity of the spectral representation is assessed by examining the convergence of the method, and comparing with the fully two-dimensional finite-volume solution (FLUENT), and the widely used depth-averaging method from shallow-water theory. It is found that a low number of modes are usually sufficient to secure convergence and accuracy. Good agreement is obtained between the low-order description and the finite-volume solution at low to moderate modified Reynolds number. The depth-averaging solution is unable to predict accurately (qualitatively and quantitatively) the high-inertia flow. The influence of inertia is examined on the flow. Copyright © 2003 John Wiley & Sons, Ltd.

KEY WORDS: spectral/finite difference scheme; narrow-channel flow; inertial flow; lubrication

1. INTRODUCTION

Thin-film flow is encountered in the processing industry, particularly in lubrication, die flow, coating, injection molding, and die casting. The understanding of the flow inside a channel of arbitrary shape for high-inertia flow remains challenging, despite the continuous development of new solution techniques and the advent of powerful computational platforms. The presence of geometrical non-linearities, coupled with material non-linearities such as inertia (high-speed lubrication, and die casting) and non-Newtonian effects (injection molding), makes the

* Correspondence to: R. E. Khayat, Department of Mechanical and Materials Engineering, The University of Western Ontario, London, Ontario, Canada N6A 5B9.
† E-mail: rkhayat@eng.uwo.ca

Contract/grant sponsor: Natural Sciences and Engineering Research Council of Canada.
Contract/grant sponsor: Ontario Ministry of Training, Colleges and Universities.

Received 30 October 2002
Revised 22 January 2003

problem difficult to investigate. The problem can be reduced by one dimension by implementing the Hele-Shaw or lubrication approximation for thin films [1]. Although the lubrication assumption remains the basis for the simulation of flow of thin films, it is mostly used with inertia effects neglected [2]. The handling and understanding of inertia effects is precisely the object of the present study.

The influence of inertia in lubrication and die casting problems has been addressed in several studies [3–9]. In classical lubrication theory, the Navier–Stokes equations are reduced to the Reynolds equation under the assumption that the inertia forces are negligible compared to the viscous forces. Recently, the need to include inertia effects has arisen because of the increasing number of lubrication flow at moderately large Reynolds numbers [8]. Such applications include large size bearing operating with conventional lubricants, bearings and seals operating with non-conventional lubricants such as liquid metals and water, and the use of high-speed bearings. In these cases, it is imperative to extend the Reynolds equation [1] to include inertial effects. Chen and Chen [3] have reported that the influence of fluid inertia in journal bearings can exceed 10% in terms of load. In the case of uni-directionally loaded slider bearings, load capacity increases in direct proportion to Re; the increase being around 4% for $Re = 1000$ and around 1% for $Re = 1$ [4]. In die casting, inertia effects are clearly dominant. The molten metal is injected into the die cavity under high pressure and velocities for reduced cycle times. Typical filling times are on the order of 40 ms and the Reynolds number could be as high as 10 000 [5]. Therefore, common simplifications used for modelling less complex flow problems in casting and high-speed lubrication flow, such as the assumption of viscous dominated flow are not valid. The inclusion of inertia is thus essential for any fluid flow model used in die casting and high-speed lubrication. However, the handling of convective non-linearities presents major challenges in thin-film flow.

Although the lubrication formulation reduces the pressure to its hydrostatic part, thus eliminating the momentum equation in the depthwise direction from the problem, the dimension of the problem remains the same as the original equations. Benney's long-wave (LW) approximation [10] is often used, especially for low-inertia flow. At high Reynolds number, inertia is better accounted for through the 'boundary-layer' (BL) approximation, which includes the effect of transverse flow and the convective terms. Salamon *et al.* [11] carried out a finite-element solution of the full Navier–Stokes equations for the flow in a falling film. Comparison of their results with those based on the LW approximation, indicates that serious limitations exist in the validity of the LW equation. The major difference between the original Navier–Stokes equations and the BL equations is the hydrostatic variation of the pressure across the film depth. As a result, only the transverse momentum equation is eliminated, but the convective terms are retained in the remaining equations, and the number of boundary conditions is reduced. However, the solution of the BL equations remains essentially as difficult to obtain as that of the Navier–Stokes equations [12]. A depthwise integration, along z, of the momentum equation(s) in the lateral direction(s), along x (and y) is usually performed by assuming a self-similar semi-parabolic flow profile in the z-direction, as was proposed by Shkadov [13]. Although the depth-averaged equations are only of second order in time, they yield plausible results, at least qualitatively, but they remain fundamentally questionable because of the semi-parabolic assumption [14, 15]. The parabolic approximation is widely used in the literature, and its validity was established experimentally by Aleksenko *et al.* [17] for thin-film flow. However, it is generally argued that the parabolic approximation is valid at

low or moderately-low Reynolds number, and provided the surface waves are far from the entry [18, 19]. In addition to high-inertia flow, other flow conditions that restrict the range of validity of the semi-parabolic profile include the presence of end effects, turbulent flow, and (most likely) nonlinear effects stemming from shear-thinning or viscoelastic effects [20, 21]. A more rigorous approach for the solution of the thin-film equations becomes almost as difficult to achieve as for the original Navier–Stokes equations. Hence, conventional solution techniques such as the finite-element or finite-difference methods are not suitable given the rapid spatio-temporal variation of the flow field in the presence of steep waves. Frequent remeshing, and an effective implicit time-stepping scheme are required. Ruyer-Quil and Manneville [22] used a three-term expansion of the flow field in the transverse direction, and obtained three coupled equations for the surface height, flow rate and stress. Takeshi [12] examined the flow in a falling film at moderate Reynolds number and large but finite Weber number, using a regularization method, which consists of a combination of the Pade approximation and the long-wave expansion. More recently, Khayat [23, 24] proposed a formal spectral approach for transient thin-film flow, whereby the velocity is expanded in terms of orthonormal functions in the depthwise direction. A hierarchy of equations is obtained using the Galerkin projection. Comparison led to excellent agreement with Watson's similarity solution [16]. Given the importance of inertia upon inception, the BL formulation rather than Benney's LW approximation [10] was used. The flow equations were first mapped over the rectangular domain, and a formal expansion of the velocity field in terms of orthonormal basis functions is introduced for the flow field. The formulation closely follows and generalizes that of Zienkiewicz and Heinrich [25], which emphasizes water flow over extended areas.

In this paper a hybrid spectral/finite-difference methodology is developed to solve the boundary-layer equations for a flow inside a channel of varying depth. The method consists of expanding the flow field in a finite series of known global, smooth orthogonal functions in the streamwise and depthwise directions. The problem formulation is given in Section 2, where the lubrication equations are briefly reviewed. The solution procedure is outlined in Section 3. Results are given in Section 4, where convergence is assessed, and comparison with results based on fully two-dimensional flow is carried out. Finally, concluding remarks are given in Section 5.

2. GOVERNING EQUATIONS AND BOUNDARY CONDITIONS

Consider the two-dimensional flow inside a cavity of a viscous, Newtonian and incompressible fluid, of density ρ and viscosity μ. The two-dimensional Cartesian system of coordinates is taken as x_1 and x_2, with the x_1 and x_2 axis lying in the streamwise and depthwise direction, respectively. Let u_1 and u_2 be the corresponding velocity components, and P the pressure. The flow is driven by a constant pressure gradient maintained inside the straight channel portion upstream, of depth D. Gravity is assumed to be negligible. The flow is assumed to be symmetric with respect to the x_1 axis, resulting from the symmetry in flow conditions and channel shape, $x_2 = H(x_1)$. The governing equations are cast in terms of dimensionless variables. Typically, in two-dimensional thin-channel flow, there are two characteristic lengths, L, along x_1, and D along x_2. The reference, V, is taken as the maximum velocity inside the

straight channel. The dimensionless variables are introduced as follows:

$$(x, y) = \left(\frac{x_1}{L}, \frac{x_2}{\varepsilon L}\right), \quad (u, v) = \left(\frac{u_1}{V}, \frac{u_2}{\varepsilon V}\right), \quad h = \frac{H}{D}, \quad p = \varepsilon^2 \frac{L}{\mu V} P \tag{1}$$

Two important dimensionless groups emerge in the problem, namely, the Reynolds number, Re, and the aspect ratio, ε:

$$Re = \frac{\rho V L}{\mu}, \quad \varepsilon = \frac{D}{L} \tag{2}$$

In dimensionless form, and if terms of $O(\varepsilon^2)$ and higher are excluded, the governing equations for steady-state flow reduce to:

$$u_x + v_y = 0 \tag{3}$$

$$\varepsilon^2 Re(uu_x + vu_y) = u_{yy} - p_x \tag{4a}$$

$$p_y = 0 \tag{4b}$$

where a subscript denotes partial differentiation. The parameter $\varepsilon^2 Re = \delta$ is often referred to as the modified Reynolds number [1]. Equations (3) and (4) are of the boundary-layer type. They simply state that the depth variation of the pressure is negligible, and the elongational diffusive term is dominated by the shear term. Note that δ is not necessarily negligible since Re may be large enough for this term to be of order one. In this work, Re is assumed to be $O(1/\varepsilon^2)$. If the modified Reynolds number is very small, i.e. Re is of $O(1)$, then all non-linear terms can be neglected, which will represent creeping flow of viscous fluids. In that case, Equation (4) reduces to Reynolds equation in lubrication theory [1]. In this work, the flow inside thin (symmetric) channels of arbitrary shape will be examined. Thus, the domain of computations for Equation (4) is given by $(x, y) \in [0, 1] \times [0, h(x)]$. Although the combination $\varepsilon^2 Re$ may be treated as a similarity parameter, it is convenient to refer to ε and Re as two separate similarity parameters, as indeed is the case when comparison with the fully two-dimensional flow is carried out.

The no-slip and no-penetration boundary conditions at the upper boundary give

$$u(x, y = h) = v(x, y = h) = 0 \tag{5a}$$

while the symmetry conditions lead to

$$u_y(x, y = 0) = v(x, y = 0) = 0 \tag{5b}$$

The flow is assumed to be driven by an imposed axial velocity $U_0(y) = U(x = 0, y)$ at the channel entrance. Thus, the general boundary condition at the entrance to the cavity is given by

$$u(x = 0, y) = U_0(y) \tag{5c}$$

At $x=1$, the fluid is assumed to exit the channel under atmospheric condition so that

$$p(x=1)=0 \tag{5d}$$

System (3)–(4) is next solved subject to boundary conditions (5).

3. SOLUTION PROCEDURE

In this section, the problem is solved using a spectral expansion for velocity and pressure. The depth-averaging method is also used for comparison, and will be outlined as well.

3.1. Spectral expansion

The problem is solved by expanding the velocity components $u(x, y)$ and $v(x, y)$ in terms of appropriate orthogonal functions, and using the Galerkin projection method to obtain a set of ordinary differential equations (ODEs) that govern the expansion coefficients. The expansion coefficients are then determined using finite-difference method. Given the symmetry of the flow, Equation (4) clearly indicates that only a symmetric flow is admissible. Hence, $u(x, y)$ and $v(x, y)$ are expanded as

$$\begin{aligned} u(x,y) &= \sum_{n=0}^{\infty} u_n(x)\cos\left[(2n+1)\frac{\pi y}{2h}\right] \\ v(x,y) &= \sum_{n=0}^{\infty} v_n(x)\sin\left[(n+1)\frac{\pi y}{h}\right] \end{aligned} \tag{6}$$

where $u_n(x)$ and $v_n(x)$ are the expansion coefficients. The above expressions of u and v satisfy the boundary conditions ((5a) and (5b)). Obviously, a truncation level will have to be imposed, leading to a finite number of modes, M, in the expansion.

The expressions for u and v are substituted in Equation (3) and the Galerkin projection method is used, which consists of multiplying Equation (3) by $\sin[(m+1)\pi y/h], m \in [0, M]$, and integrating with respect to y from $-h$ to h. The following expression is then obtained for the expansion coefficient v_m, namely

$$v_m(x) = -\frac{h(x)}{\pi^2(m+1)}\sum_{n=0}^{M}\left[\frac{\sin(n-m-1/2)\pi}{(n-m-1/2)} + \frac{\sin(n+m+3/2)\pi}{(n+m+3/2)}\right]u_n'(x) \tag{7}$$

Similarly, after applying the Galerkin projection for the x-momentum equation (4) and substituting the expression for v_m, the following relation is obtained:

$$u_k(x) = A_k\, p_x + \sum_{m=0}^{M}\sum_{n=0}^{M} B_{kmn}u_m'u_n \tag{8}$$

where

$$A_k = -\frac{16(-1)^k h^2}{[\pi(2k+1)]^3}$$

and

$$B_{kmn} = \frac{4\delta h}{[\pi(2k+1)]^2}\left\{\left\langle -\cos\left[\frac{(2n+1)\pi y}{2h}\right]\cos\left[\frac{(2m+1)\pi y}{2h}\right]\cos\left[\frac{(2k+1)\pi y}{2h}\right]\right\rangle + \frac{1}{2}\sum_{p=0}^{M}\frac{(2n+1)}{\pi(p+1)}\left\langle \sin\left[\frac{(p+1)\pi y}{h}\right]\sin\left[\frac{(2n+1)\pi y}{2h}\right]\cos\left[\frac{(2k+1)\pi y}{2h}\right]\right\rangle \times\left[\frac{\sin(m-p-1/2)\pi}{(m-p-1/2)}+\frac{\sin(m+p+3/2)\pi}{(m+p+3/2)}\right]\right\}$$

The notation $\langle\,\rangle$ indicates integration over the interval $y\in[-h,h]$. The system of Equations (7)–(8) along with the boundary condition (5) is a well-posed problem if p_x is known. However, the pressure remains one of the unknown in the system, and an additional equation is needed. This equation is based on the constancy of the volume flow rate. In dimensionless form, one has

$$\int_0^h u(x,y)\,\mathrm{d}y = \frac{2}{\pi}h(x)\sum_{n=0}^{M}\frac{(-1)^n u_n(x)}{2n+1} = \frac{1}{3} \tag{9}$$

Although mass conservation is ensured through the continuity equation, Equation (9) is still needed as the volume flow rate is actually prescribed. Thus, there are $M+2$ unknowns in the system, namely, the velocity coefficients and the pressure gradient. One of the unknowns, $u_0(x)$, is eliminated, in terms of the remaining coefficients, by substituting expression (6) into Equation (9). Hence,

$$u_0(x) = \frac{1}{6\pi h} - \sum_{n=1}^{M}\frac{(-1)^n u_n}{2n+1} \tag{10}$$

Upon substituting expression (10) into Equation (8) for $k=0$, one obtains an expression for p_x in terms of u_n for $n\in[1,M]$. In this manner, the pressure gradient is eliminated in terms of the M velocity coefficients, using the first equation in (8), namely that corresponding to $k=0$. These unknown coefficients are determined by solving the set of M equations resulting from system (8), which can be recast as a set of first-order coupled ODEs for the coefficient, $u_{n\geqslant 1}(x)$, with the first-order derivatives given explicitly in terms of the lower-order terms. The boundary conditions at $x=0$ for system (8) are deduced from (5b), leading to:

$$u_n(x=0) = \frac{1}{h}\int_{-h}^{+h} U_0(y)\cos[(2n+1)\pi y/2h]\,\mathrm{d}y, \quad v_n(x=0)=0 \tag{11}$$

Note that for the present problem, $U_0(y)=1-4y^2$. The problem thus reduces to an initial-value problem, which is solved using the Runge–Kutta–Verner method (IMSL-DIVPRK). The sub-routine DIVPRK finds an approximation to the solution of a system of first-order ordinary differential equations for given initial data. The sub-routine attempts to keep the global error proportional to a user-specified tolerance. A step size (Δx) less than 0.01 was used to maintain a tolerance of 10^{-7}.

3.2. *Depth-averaging method*

This method is based on a parabolic representation of the streamwise velocity, which is solution that is strictly valid for a flow with zero inertia. An approach, which has been widely used in the literature, is to maintain a parabolic representation for u even if inertia is not negligible. The method consists of averaging out the inertia effects across the film. Upon using boundary conditions (5a) and (5b) on u, as well as condition (9) on the flow rate, one has

$$u(x, y) = -\frac{1}{2h^3}(y^2 - h^2) \tag{12}$$

In this case, the depthwise velocity component is determined upon integrating the continuity equation, which gives

$$v(x, y) = -\frac{h'}{2h}\left[\left(\frac{y}{h}\right)^3 - \frac{y}{h}\right] \tag{13}$$

Although the continuity equation as well as the boundary conditions (5) by expressions (12) and (13), the momentum equation (4a) can only be satisfied in the average sense. Thus, the pressure becomes dictated by the following equation:

$$\varepsilon^2 Re\, h^2 \left[\int_0^h (uu_x + vu_y)\, \mathrm{d}y\right] = 1 - h^3 p_x \tag{14}$$

In the limit of negligible inertia, Equation (14) reduces to the Reynolds equation for the pressure [1].

4. RESULTS AND DISCUSSION

The methodology above is now applied for the steady-state flow in Figure 1. The convergence is first examined. The validity of the spectral representation is then assessed upon comparison with the finite-volume method. Comparison against the depth-averaging method is also carried out. Once the numerical accuracy is established, results on the influence of inertia are given. The cavity is assumed to be symmetrically modulated, with the wall shape given by $h(x) = [1 + A\sin(2\pi x/\lambda)]/2$. Here, A and λ are the (dimensionless) modulation amplitude and wavelength, respectively (in units of D). The flow upstream, at channel entrance, is assumed to be fully

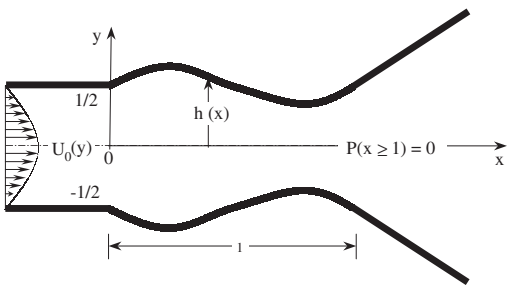

Figure 1. Computational domain in the (x, y) plane, and dimensionless notation.

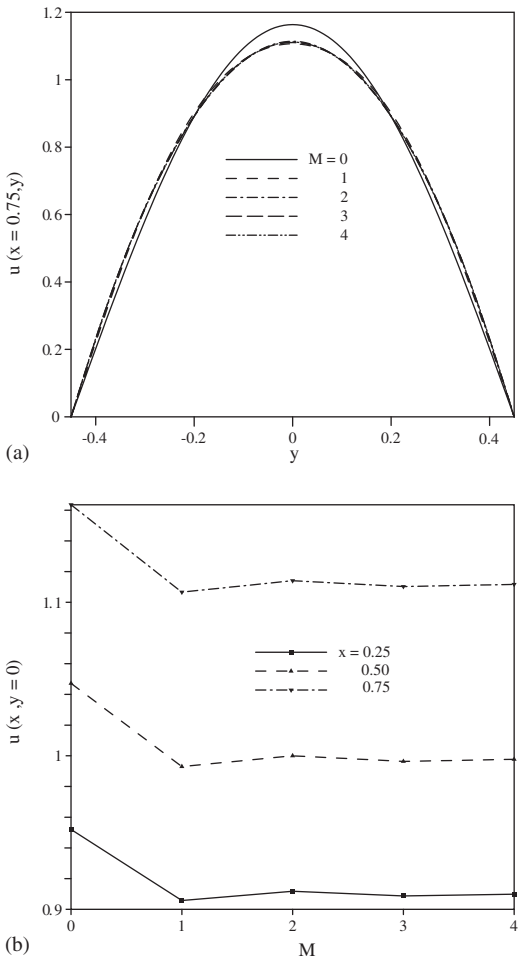

Figure 2. Convergence assessment and the influence of the number of modes on the streamwise flow for $\varepsilon = A = 0.1$, $\lambda = 1$ and $Re = 10$. The figure shows (a) the u profiles across the gap at $x = 0.75$, for $M \in [0, 4]$, and (b) the rate of convergence of the velocity at the channel centre at different locations $x \in [0.25, 0.75]$.

developed, of the Poiseuille type. In this case, the streamwise velocity at the inlet is given by $U_0(y) = 1 - 4y^2$. In order to ensure full flow development, an extended length of the straight portion of the cavity is added upstream of the modulated portion (see Figure 1). The added entrance length is estimated to be equal $0.06\varepsilon Re$ [26], for laminar flow. Note that εRe gives a Reynolds number that is based on the width of the channel. Thus, the domain of computation is taken as $(x, y) \in [-0.06\varepsilon Re, 1] \times [-h(x), h(x)]$. All results are given in dimensionless quantities.

Consider the flow corresponding to $\varepsilon = A = 0.1$, $\lambda = 1$ and $\delta = 1$. The convergence of the flow field is assessed by varying the number of modes over the range $M \in [0, 4]$. The rate of convergence is typically illustrated in Figure 2.

Table I. The convergence of the streamwise velocity tip at different axial locations for $\varepsilon = A = 0.1$, $\lambda = 1$ and $\delta = 1$.

M	$x = 0.25$	$x = 0.50$	$x = 0.75$
0	0.95199	1.04719	1.16355
1	0.90571	0.99296	1.10663
2	0.91178	0.99999	1.11407
3	0.90868	0.99637	1.11027
4	0.90982	0.99771	1.11168

The streamwise velocity distributions across the gap at $x = 0.75$ are shown in Figure 2a. The coarsest result corresponds to the inclusion of only one mode ($M = 0$), which tends to overestimate the streamwise velocity at the centre, and slightly underestimate it elsewhere. Convergence is essentially attained for $M \geqslant 3$. The fast rate of convergence is clearly reflected in Figure 2(b) and in Table I, where the velocity tip is plotted against M at three different axial locations, for the same conditions as in Figure 2(a). Similar rates of convergence are obtained for the velocity at other y locations. The velocity drops sharply from $M = 0$ to $M = 1$ for all three locations, and the effect of the number of modes becomes increasingly smaller as M increases. The velocity remains essentially unchanged for $M \geqslant 3$. It is important to emphasize that the above figures indicate that the convergence of the streamwise velocity is uniform throughout the gap.

A somewhat slower rate of convergence is found when the depthwise velocity component is examined. The results are summarized in Figure 3. When only one mode is retained ($M = 0$), the depthwise flow is essentially non-existent, $v(x, y) = 0$. Similarly to streamwise flow, convergence is attained for $M \geqslant 3$, as shown in Figure 3(a). The absolute maximum depthwise velocity tends to increase with M, and its location shifts slightly towards the centreline ($y = 0$). Figure 3(b) shows the absolute maximum value and its location plotted against the number of modes at $x = 0.75$. There is a significant jump for M small, with a slight overshoot at $M = 2$. The rate of convergence of the location of the maximum/minimum is slightly faster, as indicated by the leveling in Figure 3(b). Finally, additional calculations show that the rate of convergence displayed in Figures 2 and 3 is typical of any Reynolds number in the moderate range. Consequently, the results reported below are based on $M = 3$.

The convergence assessment above gives only an estimation of the relative error of the formulation and numerical implementation. That is, the solution may very well converge when higher-order modes are added, but the question remains as to whether the solution has converged to the exact value. In order to estimate the absolute error of the proposed methodology, the results are compared against the results based on a fully two-dimensional finite-volume method, using the FLUENT software package. Comparison with the two-dimensional flow is important as it allows the assessment of the error resulting from the lubrication approximation. The boundary conditions used in FLUENT are Poiseuille flow conditions upstream at the entrance to the flow domain, and zero diffusion flux for all flow variables with an overall mass balance correction at the exit. An extrapolation procedure is used by FLUENT, which updates the outflow velocity and pressure in a manner that is consistent with fully-developed flow between parallel plates.

Comparison against the depth-averaging method is also conducted. This method is widely used in the literature, whereby the streamwise velocity is assumed to be parabolic across the

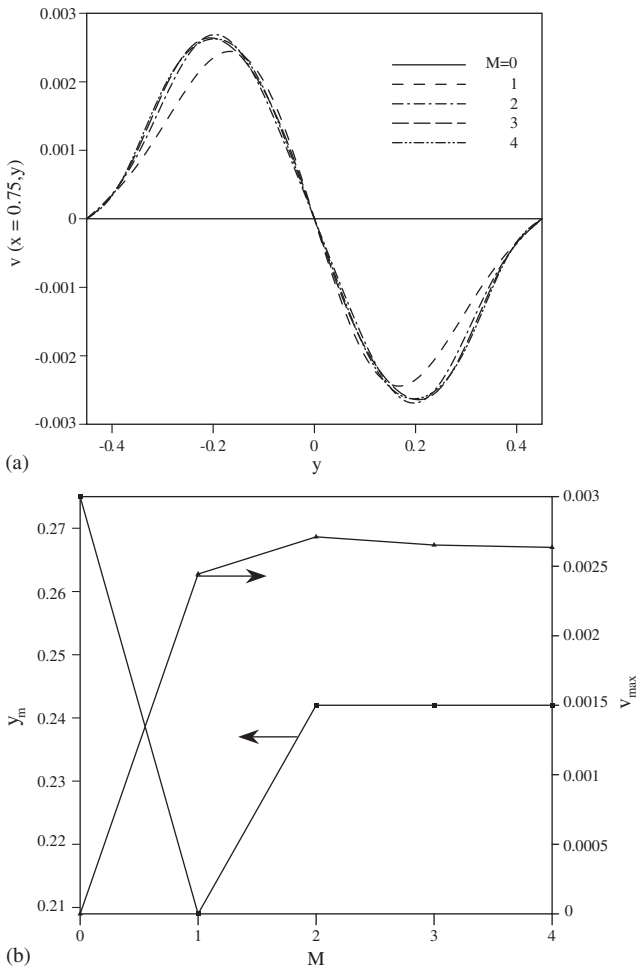

Figure 3. Convergence assessment and influence of the number of modes on the depthwise flow for $\varepsilon = A = 0.1$, $\lambda = 1$ and $Re = 10$. The figure shows (a) the v profiles across the gap at $x = 0.75$, for $M \in [0, 4]$, and (b) the rate of convergence of the maximum depthwise velocity, $v_{\max}$, and its location, y_{m}.

gap. This assumption leads to an exact solution in the absence of inertia, and has been adopted for non-zero Reynolds number flow. However, the parabolic profile is only valid when inertia is not significant ($Re < 500$) (see, for instance, Reference [24]).

Comparison among the three methods is typically illustrated in Figure 4, where the streamwise and depthwise velocity profiles are plotted against the lateral position, y, for $\varepsilon = A = 0.1$, $\lambda = 1$ and $\delta = 1$, at axial location $x = 0.75$. The results illustrate the situation for low-Reynolds-number flow. The figure clearly indicates that agreement is excellent among the three methods concerning the streamwise velocity component (Figure 4(a)). However, there is considerable discrepancy in the case of the depthwise velocity component (Figure 4(b)). The solution from the depth-averaging method is negligibly small (essentially zero). There is a small difference

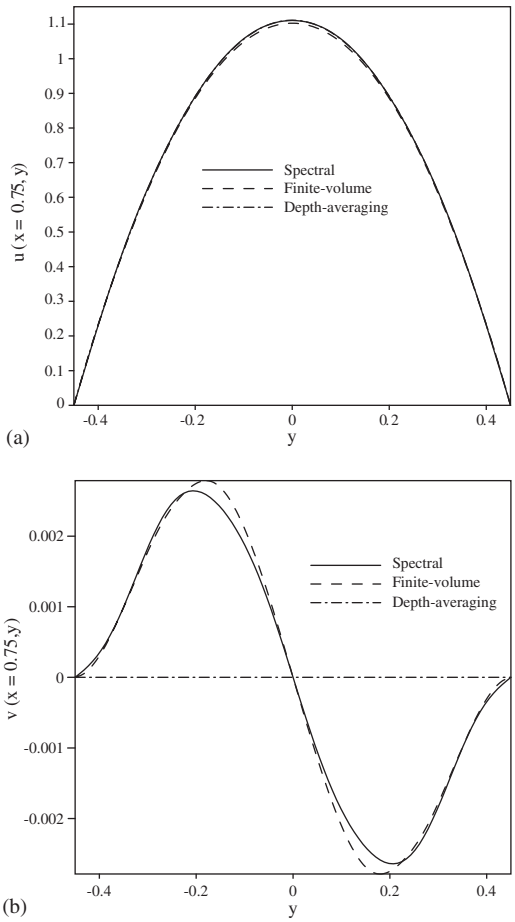

Figure 4. Comparison among the spectral, finite-volume, and the depth-averaging methods for low-inertia flow, for $\varepsilon = A = 0.1$, $\lambda = 1$ and $Re = 10$. The figure shows (a) the u profiles, and (b) the v profiles, across the gap at $x = 0.75$.

(on the order of 3%) between the spectral and finite-volume solutions, particularly near the extrema. The current formulation tends to underestimate slightly the buildup of depthwise flow.

Figure 5 shows the velocity profiles from the three different schemes at higher modified Reynolds number, $\delta = 100$, at axial location $x = 0.25$. The depth-averaging method is unable to reflect the effect of inertia, which can be noticed from the figure and is a major drawback of this method. The spectral method represents the inertia effect very well and results agree closely with finite-volume (FV) solution.

The issue regarding the accuracy of the solution based on FLUENT is important to examine, as this solution is taken as 'exact'. Since the flow is steady, only the mesh size influences the solution. In this case, the calculations were carried out on a PC with Pentium III processor, 550 MHz. The FV method used in FLUENT consists of integrating the fully two-dimensional conservation equations (as opposed to the approximate boundary-layer equations used in the

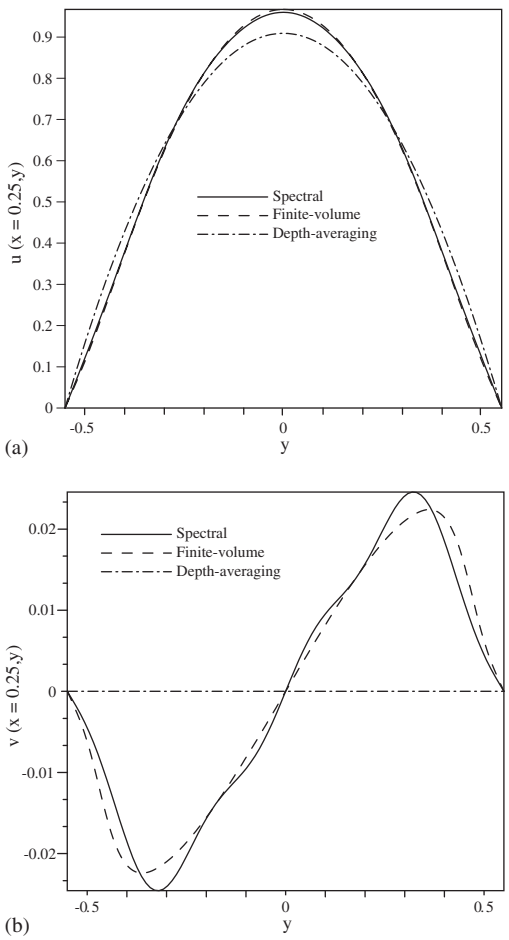

Figure 5. Comparison among the spectral, finite-volume, and the depth-averaging methods for high-inertia flow, for $\varepsilon = A = 0.1$, $\lambda = 1$ and $Re = 1000$. The figure shows (a) the u profiles, and (b) the v profiles, across the gap at $x = 0.25$.

present formulation) over each control volume ensuring conservation over each control volume. Central values for the velocity and pressure are stored, and values at the faces are interpolated. This is accomplished using a first-order upwind discretization scheme. The grid used in FLUENT is unstructured and is generated by mesh generation software GAMBIT. In this case, FLUENT uses internal data structures to assign an order to the cells, faces, and grid points in a mesh, and to maintain contact between adjacent cells.

The streamwise and depthwise velocity profiles are shown in Figure 6 for different mesh sizes. The spectral solution is also included for reference. The streamwise velocity increases at any y location as the mesh is refined (Figure 6(a)), with a reasonably fast rate of convergence. The rate of increase of the velocity is higher near the centre than elsewhere. The finite-volume solution tends to generally underestimate the strength of streamwise flow. More importantly, the finite-volume solution appears to converge toward the spectral profile with

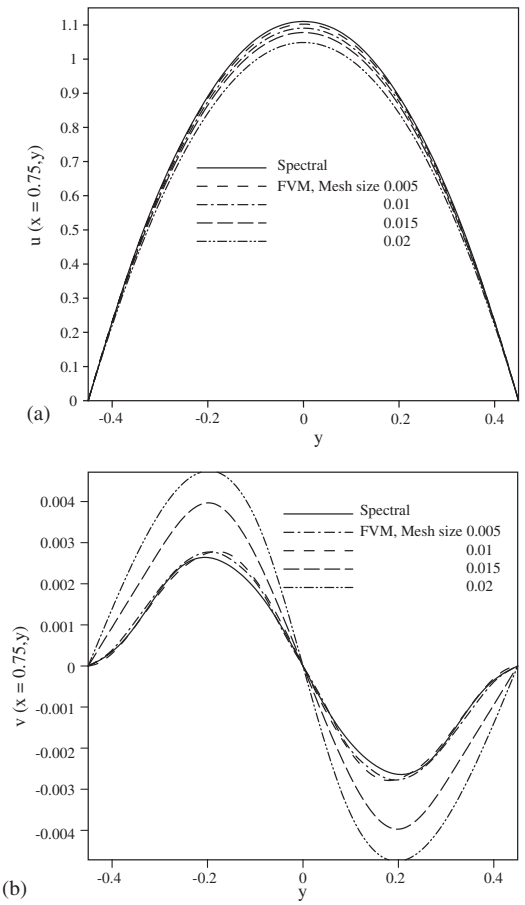

Figure 6. Influence of mesh size on the finite-volume results for $\varepsilon = A = 0.1$, $\lambda = 1$ and $Re = 10$. The figure shows (a) the u profiles, and (b) the v profiles, across the gap at $x = 0.75$. The spectral profiles are also included for reference.

mesh refinement. In contrast, the depthwise velocity is generally overestimated by the finite-volume method (Figure 6(b)), and is less accurate than the streamwise velocity prediction for the cruder mesh sizes. However, it is clear from the figure that the rate of convergence is fast, and there is excellent agreement with the spectral solution.

Regarding CPU and storage requirements, these have also been assessed. It is obvious that the low-dimensional spectral scheme proposed requires little storage on any computational platform. It is also found that the CPU time to solve the problem by FLUENT is typically around 30 min (excluding pre- and post-processing time), compared to only 3–4 min for the spectral solution.

Finally, now that the accuracy of the method is fully established, it is useful to explore the effect of inertia on the flow. This is done by varying the modified Reynolds number. The velocity profiles for different δ are shown in Figure 7 at $x = 0.25$. The streamwise velocity component increases slightly near the centre and decreases slightly elsewhere as shown in

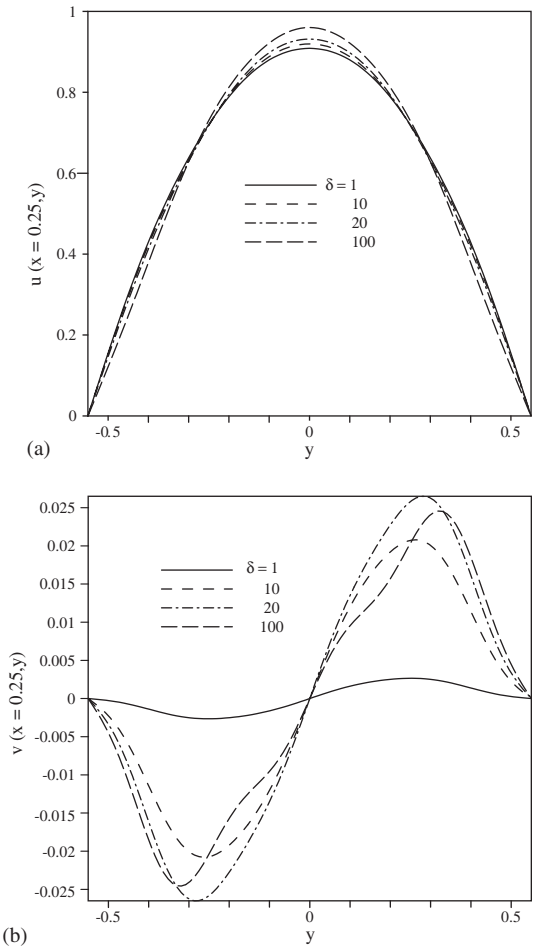

Figure 7. Influence of inertia for $\varepsilon = A = 0.1$ and $\lambda = 1$. The figure shows (a) the u profiles, and (b) the v profiles, across the gap at $x = 0.25$, for $\delta \in [1, 100]$, where $\delta = \varepsilon^2 Re$.

Figure 7(a). There is relatively little qualitative change, other than the profile deviating away from parabolic as inertia increases. In contrast, inertia seems to have a more significant influence on the depthwise flow (Figure 7(b)). The effect on the change in velocity is much more pronounced between $\delta = 1$ to 10, than $\delta = 10$ to 20, which is almost 4 times larger.

5. CONCLUSION

A hybrid low-order spectral method, along with a variable-step finite-difference discretization, is proposed to solve a wide class of lubrication problems, with inertia effects. The general lubrication formulation is applied to the flow inside a (two-dimensional) symmetric channel of arbitrary thickness. The validity of the approach is assessed upon comparison with the

finite-volume and depth-averaging method. The influence of inertia is also examined. The study shows that the low-order spectral representation in the depthwise direction can handle non-linearity with good accuracy. The accuracy of the solution depends on the number of modes, and in this study the solution converges after only a few modes. Thus, the spectral representation is particularly effective in this case since, in thin-film flow, the variation of the flow field in the depthwise direction is not expected to be strong. The solution agrees very well with the finite-volume solution (FLUENT) at low to moderate modified Reynolds number, whereas the widely used depth-averaging method fails even at moderate modified Reynolds number. The streamwise velocity increases at the centre ($y = 0$) and decreases slightly elsewhere with inertia. The proposed method requires little storage and one-tenth of CPU time than finite-volume software package.

This study is fundamentally important, as it establishes an effective solution methodology that handles non-linear flow in lubrication problems. Potential extensions include non-Newtonian flows, namely when shear-thinning and viscoelastic effects are incorporated, as well as other flow geometry.

ACKNOWLEDGEMENTS

The support of the Natural Sciences and Engineering Research Council of Canada is gratefully acknowledged. MRS has also benefited from the support of the Ontario Ministry of Training, Colleges, and Universities.

REFERENCES

1. Hamrock BJ. *Fundamentals of Fluid Film Lubrication*. McGraw-Hill: New York, 1994.
2. Agassant JF, Avens P, Sergent JPh, Carreau PJ. *Polymer Processing*: *Principles and Modeling*. Hanser Publishers: Munich, 1991.
3. Chen C, Chen C. The influence of fluid inertia on the operating characteristics of finite journal bearings. *Wear* 1989; **131**:229.
4. Chen PYP, Hahn EJ. Use of computational fluid dynamics in hydrodynamic lubrication. *Journal of Engineering and Tribology* 1998; **212**:427.
5. Venkatesan K, Shivpuri R. Numerical simulation and comparison with water modeling studies of the inertia dominated cavity filling in die casting. In *Simulation of Materials Processing*: *Theory*, *Methods and Applications*. Shen SF, Dawson PR (eds). Balkema Publishers:Rotterdam, 1995; 1203.
6. Kheshgi HS. Profile equations for film flows at moderate Reynolds numbers. *AIChE Journal* 1989; **35**:1719.
7. Tuck EO, Bentwich M. Sliding sheets: lubrication with comparable viscous and inertia forces. *Journal of Fluid Mechanics* 1983; **135**:51.
8. Oron A, Davis SH, Bankoff SG. Long-scale evolution of thin liquid films. *Reviews in Modern Physics* 1997; **69**:931.
9. Wilson SK, Duffy BR. On lubrication with comparable viscous and inertia forces. *Quarterly Journal of Mechanics and Applied Mathematics* 1998; **51**:105.
10. Benney DJ. Long waves in liquid films. *Journal of Mathematics and Physics* 1966; **45**:150.
11. Salamon TR, Armstrong RC, Brown RA. Traveling waves on vertical films: numerical analysis using the finite-element method. *Physics of Fluids*, 1994; **6**:2202.
12. Takeshi O. Surface equation of falling film flows with moderate Reynolds number and large but finite Weber number. *Physics of Fluids* 1999; **11**:3247.
13. Shkadov VY. Wave conditions of a flow in a thin viscous layer under the action of gravitational forces. *Izvestiya Akademii Nauk SSSR, Mekhanika Zhidkosti i Gaza* 1967; **1**:43.
14. Prokopiou T, Cheng M, Chang HC. Long waves on inclined films at high Reynolds number. *Journal of Fluid Mechanics* 1991; **222**:665.
15. Chang HC. Wave evolution on a falling film. *Annual Review of Fluid Mechanics* 1994; **26**:103.
16. Watson EJ. The radial spread of a liquid jet over a horizontal plane. *Journal of Fluid Mechanics* 1964; **20**:481.
17. Aleksenko SV, Nakoryakov VV, Pokusaev BG. Wave formation on a vertical falling liquid film. *AIChE Journal* 1985; **31**:1446.

18. Wilkes JO, Nederman RM. The measurement of velocities in thin film of liquid. *Chemical Engineering Science* 1962; **17**:177.
19. Bertschy JR, Chin RW, Abernathy FH. High-strain-rate free-surface boundary-layer flows. *Journal of Fluid Mechanics* 1993; **126**:443.
20. Khayat RE. Transient free-surface flow inside thin cavities of viscoelastic fluids. *Journal of Non-Newtonian Fluid Mechanics* 2000; **91**:15.
21. Khayat RE. Transient two-dimensional coating flow of a viscoelastic fluid film on a substrate of arbitrary shape. *Journal of Non-Newtonian Fluid Mechanics* 2000; **95**:199.
22. Ruyer-Quil C, Manneville P. Modeling film flows down inclined planes. *European Journal of Physics B* 1998; **6**:277.
23. Khayat RE, Welke S. Influence of inertia, gravity and substrate topography on the transient coating flow of a thin fluid film. *Physics of Fluids* 2001; **13**:355.
24. Khayat RE. Influence of inertia on the transient axisymmetric free-surface flow inside thin cavities of arbitrary shape. *Physics of Fluids* 2001; **13**:3636.
25. Zienkievicz OC, Heinrich JC. A unified treatment of steady-state shallow water and two-dimensional Navier-Stokes equations—finite-element penalty function approach. *Computer Methods in Applied Mechanics and Engineering* 1979; **17**/**18**:673.
26. White FM. *Fluid Mechanics* (4th edn). McGraw-Hill: New York, 1999.

